Two-Path Impedance Spectroscopy for Measuring Paracellular and Transcellular Epithelial Resistance

Susanne M. Krug, Michael Fromm, and Dorothee Günzel*
Institute of Clinical Physiology, Charité, Campus Benjamin Franklin, Freie Universität and Humboldt-Universität, Berlin, Germany

ABSTRACT Solutes are transported across epithelial cell layers via transcellular and paracellular pathways. The transcellular pathway leads across the apical and basolateral cell membrane, whereas the paracellular pathway is directed through the tight junction. Tight junction proteins (claudins, occludin, tricellulin) can not only form barriers but also paracellular channels that are—in concert with membrane channels and transporters—regulated in a wide range in health and disease states. Thus, it is desirable to determine para- and transcellular resistance (R^{para}, R^{trans}) separately. This cannot be achieved by conventional transepithelial resistance (TER) measurements. We present an impedance spectroscopic approach that is optimized for differentiation between these two pathways. The method is based on a transepithelial impedance measurement in specialized Ussing chambers, combined with a Ca^{2+}-dependent modulation of R^{para} through EGTA and flux measurements of a nonradioactive paracellular marker, fluorescein. The prerequisites are a paracellular marker that varies in parallel to $1/R^{para}$, an experimental regime that alters R^{para} without affecting R^{trans}, and exact knowledge of the resistance of subepithelial components. The underlying prerequisites and the applicability as a routine method were verified on cell lines of different tightness including HT-29/B6 colon cells and Madin-Darby canine kidney tubule cells C7 and C11.

INTRODUCTION

The tight junction (TJ) is the main sealing site of the paracellular pathway in epithelia and many endothelia. Main components of the TJ are rows of four-transmembrane proteins residing in the apical pole of lateral cell membranes. The two extracellular loops of these proteins link to the extracellular loops from neighboring cells and by this tighten the paracellular pathway. Such TJ proteins are occludin, the family of claudins with its 24 mammalian members (1), and the recently discovered tricellulin (2). Since the discovery of TJ proteins, the focus of interest in epithelial research has shifted toward the function and contribution of the different members of the TJ protein families toward the properties of the paracellular pathway. The impact of TJ research was enhanced greatly by the finding that some TJ proteins, instead of sealing that pathway, form paracellular ion channels (e.g., claudin-2 and claudin-10b for cations, and claudin-10a for anions (3,4)). Additional attention was drawn to the ion permeability of the paracellular pathway, as pathologies of inflammatory or infectious diseases turned out to cause, or to be caused by, paracellular barrier defects (5,6).

The experimental design used most frequently in cell culture studies of TJ protein function is either an overexpression or a knock-down of the TJ protein of interest. Typically, the effect of this manipulation on the transepithelial resistance (R^t or TER) is determined and simply interpreted as paracellular effect. However, especially if stable clones of transfected cells are created without the use of a tet-on/off system, the selection process may favor clones that, unintentionally, have changed cellular properties. Furthermore, there is evidence that some TJ proteins directly or indirectly interact with ion channels (7–10), and resulting effects of such interactions may be overlooked when relying on simple R^t measurements.

Impedance spectroscopy is considered an elegant technique to investigate epithelial properties, especially in combination with modern cell biological techniques (11). It opens what we believe is a new perspective to investigations of fundamental mechanisms underlying transepithelial transport. Over the past decades, a great variety of equivalent electrical circuits with varying degrees of complexity was used in impedance studies to model epithelial properties. In the simplest lumped model (Fig. 1 *A*), epithelia are represented by three parameters: 1), an epithelial capacitance, C^{epi}; 2), an epithelial resistance, R^{epi}; and 3), a subepithelial resistance, R^{sub}. All three parameters can be determined directly from impedance spectra (12,13). Impedance spectroscopy based on this epithelial model has been applied successfully (e.g., in investigations on various inflammatory bowel diseases) to uncover barrier loss which in simple transepithelial resistance measurements is masked by a simultaneous increase in subepithelial resistance (14,15). As this method does not discriminate between the para- and transcellular pathway, it will be referred to as one-path impedance spectroscopy in this study.

In the more complex model depicted in Fig. 1 *B*, R^{epi} is represented by a paracellular (R^{para}) and a transcellular (R^{trans}) fraction. In Fig. 1 *C*, R^{trans} and C are further divided into apical (C^{ap}, R^{ap}) and basolateral (C^{bl}, R^{bl}) elements. In both cases, the equation systems derived from impedance spectroscopy are underdetermined, and therefore additional measurements are necessary to evaluate all model

Submitted May 22, 2009, and accepted for publication August 4, 2009.

*Correspondence: dorothee.guenzel@charite.de

Editor: Michael Pusch.

0006-3495/09/10/2202/10 $2.00

doi: 10.1016/j.bpj.2009.08.003

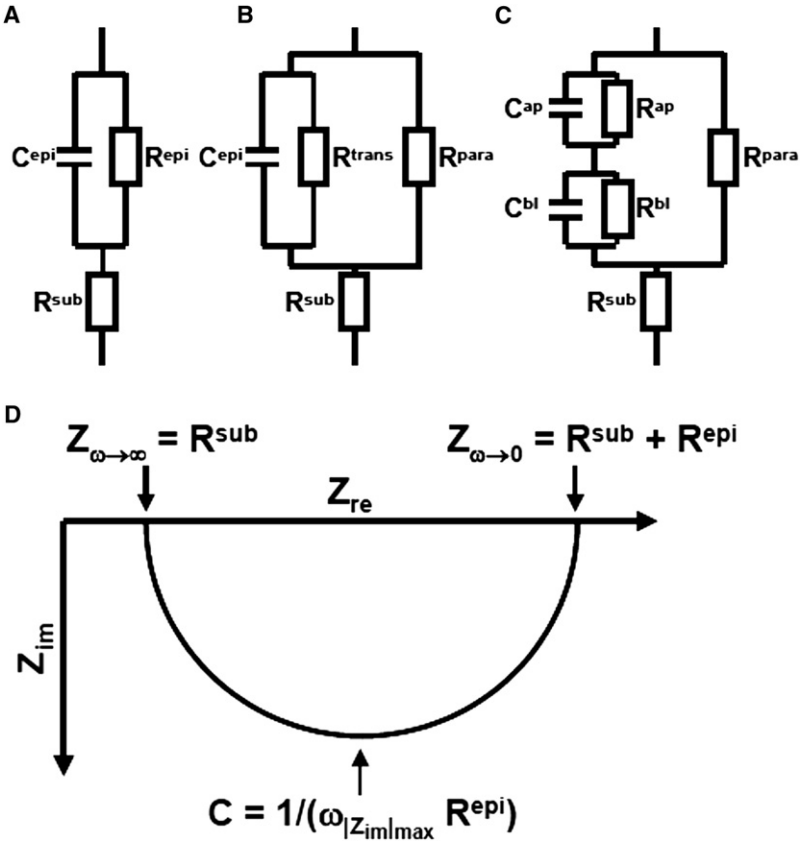

FIGURE 1 (*A*) Equivalent electrical circuit for one path impedance measurements, that only discriminate between subepithelial (R^{sub}) and epithelial (R^{epi}) resistance, and the epithelial capacity C^{epi}. (*B*) Equivalent electrical circuit for two path impedance measurements used in this study. Here, the epithelial resistance R^{epi} is composed of a paracellular (R^{para}) and a parallel transcellular (R^{trans}) resistance. Under DC conditions or AC conditions at very low frequencies $R^{epi} = R^{para} \times R^{trans}/(R^{para} + R^{trans})$. (*C*) Equivalent electrical circuit for a model discriminating between the apical (*index ap*) and the basolateral (*index bl*) side of an epithelium. In this model, the capacitance C^{epi} of the models presented in *A* and *B* is composed of C^{ap} and C^{bl} ($C^{epi} = C^{ap} \times C^{bl}/(C^{ap} + C^{bl})$. Under DC conditions or AC conditions at very low frequencies $R^{epi} = R^{para} \times (R^{ap} + R^{bl})/(R^{para} + R^{ap} + R^{bl})$. (*D*) Nyquist diagram (plot of the real and the imaginary portion of the impedance, Z_{re}, Z_{im}) for models shown in *A* and *B*. For impedance values measured at different AC frequencies, both models result in a semicircle. For high frequencies ($\omega \rightarrow \infty$) Z_{re} approaches R^{sub}, for low frequencies ($\omega \rightarrow 0$) Z_{re} approaches $R^{t} = R^{sub} + R^{epi}$. The capacitance C^{epi} can be calculated from the frequency at which $|Z_{im}|$ reaches a maximum ($C^{epi} = 1/(\omega_{|Zim|max} \times R^{epi})$. Nyquist diagrams for the model depicted in *C* only yield a semicircle, if $C^{ap}/C^{bl} = R^{bl}/R^{ap}$ (i.e., if the membrane time constant $\tau = R \times C$ is constant).

parameters. These comprise intracellular recordings to determine the plasma membrane resistance (16,17), high resolution conductance scanning (18–20) to analyze paracellular versus cellular resistances, or complete permeabilization of one cell membrane by the application of ionophores (21–23).

Even more complex models include current generating elements (transcellular active ion transport (24)), consider the lateral membrane properties in addition to discriminating between the TJ resistance and the longitudinal resistance of the paracellular cleft (distributed model (17,23)), or take into consideration that neighboring cells within a tissue may vary with respect to their electrical properties (25). However, as discussed by Bertrand et al. (26), increases in model complexity also increase the requirements for auxiliary measurements, cause longer measurement times, and necessitate the assumption that critical parameters do not change during these measurements. This last requirement can often not be met, as typical impedance scans use up to 50 discrete frequencies and individual impedance scans thus often take several minutes to completion. To overcome this problem, transient pulse measurements have been successfully applied to investigate events at high time resolution, e.g., to monitor changes in capacitance due to vesicle release (26). However, evaluation of these signals requires elaborate computations that limits a routine application of this technique.

We have developed an impedance spectroscopy-based method that is optimized for the differentiation between transcellular and paracellular pathways. The method is based on the lumped model depicted in Fig. 1 *B* and, as an auxiliary measurement that uses a reversible modulation of the paracellular pathway by the application of EGTA (calcium switch (27)) combined with flux measurements of fluorescein as paracellular marker. This method allows to determine four parameters, C^{epi}, R^{sub}, R^{trans}, and R^{para}. As it discriminates between the trans- and paracellular pathway, it will be referred to as two-path impedance spectroscopy. We show that this technique can be used successfully on various cell lines, but that its validity has to be reevaluated for each new cell line and each experimental perturbation. The method has already been applied in studies on HT-29/B6 cells (28) and Madin-Darby canine kidney (MDCK) II cells (29).

MATERIALS AND METHODS

Cell culture

Epithelial cell lines were cultured at 37°C and 5% CO_2/95% O_2 using the following culture media: HT-29/B6, RPMI 1640 (PAA Laboratories, Linz, Austria); MDCK C7 and MDCK C11, Earl's Minimal Essential Medium (PAA Laboratories); Caco-2, Earl's Minimal Essential Medium (PAA Laboratories) + GlutaMax (Gibco BRL, Karlsruhe, Germany). All culture media were supplemented with 10% (v/v) fetal bovine serum (FBS), 100 U/mL penicillin, 100 μg/mL streptomycin (Gibco BRL). For experiments, cells were seeded on filter supports (Millicell-HA, -PCF, 0.4 μm pore size, Millipore, Schwalbach, Germany) and grown to confluence within 4–6 days.

Ussing chamber and impedance measurements

Confluent cells layers on filter supports were directly mounted in conventional Ussing chambers (high resistance cell lines: HT-29/B6, MDCK C7) or glued to plastic rings with histoacryl tissue glue (30) and mounted in chambers specially designed for impedance measurements (low-resistance MDCK II cells (31)). Both hemichambers were filled with 10 mL standard bath solution (in mM: 140 Na^+, 123.8 Cl^-, 5.4 K^+, 1.2 Ca^{2+}, 1.2 Mg^{2+}, 2.4 HPO_4^{2-}, 0.6 $H_2PO_4^-$, 21 HCO_3^-, 10 D(+)-glucose, pH 7.4 when equilibrated with 5% CO_2 in O_2 at 37°C). Transepithelial potentials were clamped to 0 mV. Impedance scans were obtained as described previously (31,32), using 35 $\mu A/cm^2$ effective sine-wave alternating current at 42 discrete frequencies between 1.3 Hz and 16 kHz (high resistance cell lines) or 48 frequencies between 1.3 Hz and 65 kHz (low resistance cell lines). The resulting voltage changes were detected by phase-sensitive amplifiers (402 frequency response analyzer, Beran Instruments, Gilching, Germany; 1286 electrochemical interface, Solartron Schlumberger, Farnborough, UK), yielding complex impedance values (Z_{re}, Z_{im}) that were recorded on a computer.

Flux measurements

Flux measurements were carried out on cell layers mounted in Ussing chambers under voltage-clamp conditions. After equilibration, tracers (fluorescein-sodium salt, Sigma-Aldrich (Taufkirchen, Germany), final concentration 100 μM; FITC-dextran 10 kDa, Sigma-Aldrich, final concentration 100 μM; ^{22}Na, PerkinElmer (Weiterstadt, Germany), 2.4 kBq/mL; ^{36}Cl, Amersham (München, Germany), 10 kBq/mL) were added to the donor side (^{36}Cl, apical; ^{22}Na, fluorescein apical or basolateral) at t = zero and 1 mL (^{22}Na, ^{36}Cl) or 300 μL (fluorescein, FITC-dextran) aliquots were collected from the receiving side at t = 30, 60, and 90 min (MDCK C7 cells) or t = 10, 20, and 30 min (HT-29/B6, MDCK II cells) and immediately replaced by fresh standard bath solution. EGTA (final concentration, 1.3 mM) was added to both sides directly after collecting the third aliquot to chelate Ca^{2+} and obtain a free Ca^{2+} concentration of ~1 μM, causing R^t to decrease (Ca^{2+} switch (27)). Four further aliquots were collected at 10-min intervals after EGTA addition. Fig. S1 in the Supporting Material shows that TJs remain intact over this period of time.

Samples were analyzed in a γ-counter (^{22}Na, Wallac 1480 Wizard 3, Wallac/PerkinElmer, Weiterstadt, Germany), or after the addition of 4 mL liquid scintillate (Ultima Gold, Packard Bioscience, Dreieich, Germany) in a β-counter (^{36}Cl; Tri-Carb 2100TR, Packard Bioscience), or, as duplicates, using a 96-well plate (140 μL/well) and a plate reader (fluorescein, FITC-dextran; Spectramax Gemini, Molecular Devices, Ismaning, Germany). Fluorescence signals were calibrated using defined dilutions in standard bath saline. Flux was calculated as increase in tracer quantity (corrected for dilution) per time unit and filter area (0.6 cm^2). For direct comparison between different substances, permeabilities were calculated as flux/concentration on the donor side.

Theory

Equivalent circuits to describe epithelial properties used in this study are depicted in Fig. 1. Abbreviations used include: C, capacitance; R, resistance; G, conductance (=1/R); Z, impedance; and ω, angular frequency. Superscripts are defined as: t, total; *sub*, subepithelial; *epi*, epithelial; *trans*, transcellular; *para*, paracellular; *ap*, apical; *bl*, basolateral; *re*, real; and *im*, imaginary.

If transepithelial flux of a truly paracellular marker is measured, this flux should be directly proportional to the paracellular conductance, G^{para} (=1/R^{para}):

$$G^{para} = s \times \text{Flux}(s = \text{contant}). \quad (1)$$

Strictly, the marker flux should be corrected for the constraining effect of the filter support. However, in experiments with empty filter supports, this effect was found to be negligible. Furthermore, Eq. 1 will only hold true if the tracer molecules are small enough to pass the paracellular pores in direct proportion to the major ions that determine paracellular conductance, i.e., Na^+, Cl^-, and HCO_3^-, over the whole range of conductances tested. As shown below, this is not the case for larger molecules.

If Eq. 1 is valid for a chosen marker, then:

$$G^{epi} = G^{trans} + G^{para} = G^{trans} + s \times \text{Flux}, \quad (2)$$

with $G^{epi} = 1/R^{epi} = 1/(R^t - R^{sub})$ and $G^{trans} = 1/R^{trans}$ (model B) $= 1/(R^{ap} + R^{bl})$ (model C).

Equation 2 is a linear equation, i.e., plotting G^{epi} versus the flux of a paracellular marker should yield a straight line with the slope s and the y-intercept G^{trans} (Fig. 2 *A*). Thus, G^{trans} can be obtained directly from this graph, whereas G^{para} of the untreated cells can be calculated from slope s and the flux values obtained in the absence of EGTA, using Eq. 1.

Fig. 2, *B–D*, applies this model to various hypothetical experimental conditions. Thus, a change in G^{trans} should shift the straight line along the y axis, whereas changes in G^{para} should move the values along the straight line. In case of an undesired transcellular flux of the marker, the straight line will be shifted along the x axis, resulting in an apparent reduction of G^{trans} or even negative G^{trans} values (Fig. 2 *B*). Changes in the permeability properties reflected by a variation of s (Eqs. 1 and 2) should change the slope of the straight line, but would not disturb the calculation of G^{trans} and G^{para} (Fig. 2 *C*). Finally, an over- or underestimation of R^{sub} should distort the relationship between flux and G^{epi} and no straight line would be obtained. The effect of a constant error in R^{sub} increases with increasing G^{epi} and is therefore critical in low resistance epithelia and/or after the addition of EGTA (Fig. 2 *D*).

In summary, three prerequisites have to be fulfilled to permit the determination of the main electrical components of a cell layer: 1), use of a paracellular marker that obeys Eq. 1; 2), application of an experimental regime that

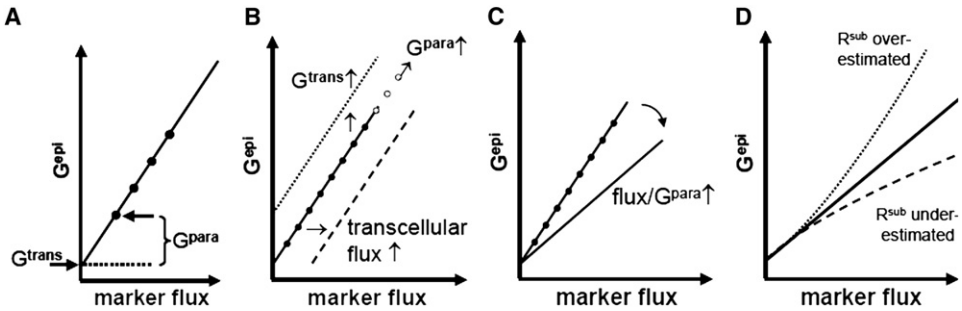

FIGURE 2 (*A*) Plotting G^{epi} versus the flux of a paracellular marker under experimental conditions that only modify the paracellular pathway yields a straight line with the slope s and the y-intercept G^{trans}. G^{para} is calculated as $s \times$ Flux. (*B*) Varying G^{trans} shifts the straight line along the y axis, whereas changing G^{para} moves the values along the straight line (*open circles*). A transcellular flux component of the marker shifts the straight line along the x axis. (*C*) Changes in the general permeability properties of the paracellular pathway affect the slope of the straight line. (*D*) Over- or underestimation of R^{sub} distorts the relationship between flux and G^{epi}.

alters R^{para} without affecting R^{trans}; and 3), an exact knowledge of R^{sub}. As all calculations presented in this study only depend on G^{epi} and the flux of a paracellular marker, they can even be applied if $C^{ap}/C^{bl} \neq R^{bl}/R^{ap}$ as depicted in the model in Fig. 1 *C*, i.e., if the Nyquist plot does not result in a semicircle (cf. Fig. 3, *B* and *D*).

RESULTS

Effect of EGTA and forskolin on the impedance of HT-29/B6 cells

In HT-29/B6 cell layers, application of both EGTA (1.3 mM) and forskolin (10 μM) cause a reduction in R^t, as detected by conventional resistance measurement. Impedance spectra, however, show not only this decrease in R^t, but also that completely different mechanisms underlie this decrease (Fig. 3). The reduction in the extracellular free Ca^{2+} concentration, $[Ca^{2+}]_o$, elicited by the application of EGTA, causes TJs to open (27,33). This reduces the diameter of the semicircle obtained in Nyquist plots from impedance scans in the absence and presence of EGTA, but essentially, the semicircular shape of the curve is retained (Fig. 3 *A*, normalized: Fig. 3 *C*). The spectra shown in Fig. 3 *A* can be used directly to determine R^{sub}, C^{epi}, and R^{epi} in the absence and presence of EGTA. In contrast, forskolin is known to activate apical cAMP-dependent Cl^- channels (34), thus reducing the transcellular resistance and changing the shape of the impedance curve in the Nyquist plot (Fig. 3 *B*, normalized: Fig. 3 *D*). In this case, the spectra shown in Fig. 3 *B* can be used to determine R^{sub} and R^{epi} in the absence and presence of forskolin, but C^{epi} can only be determined in the absence, not in the presence of forskolin, because the two minima of the curve in the presence of forskolin cannot be related directly to the apical and basolateral capacities of the cells.

Fluorescein flux versus G^{epi} in HT-29/B6 cells in the absence and presence of EGTA

When experiments like those shown in Fig. 3 are combined with flux measurements of a paracellular marker, the transepithelial conductance, G^{epi}, can be plotted against this flux, or the permeability calculated from the flux values, as described above. Fig. 4 *A* shows that, in the case of EGTA applications, this plot indeed yields a straight line with a *y*-intercept of 0.89 mS/cm^2, equivalent to R^{trans} of 1120 $\Omega \times$ cm^2. Fig. 4 *B* shows the equivalent plot for values obtained from experiments during which forskolin was applied for 30 min before applying EGTA. In these experiments, forskolin increases G^{epi} without affecting fluorescein flux, indicating that G^{trans} increased due to forskolin. The subsequent application of EGTA caused an increase in both G^{epi} and fluorescein flux, the slope of this relationship being in the same order as the slope in the absence of forskolin (*dotted line* in Fig. 4 *B*). If this result is again interpreted as an increase in paracellular conductance, then a G^{trans} value in the presence of forskolin of 3.0 mS/cm^2 can be deduced from the *y*-intercept, i.e., forskolin caused R^{trans} to decrease from 1120 to 333 $\Omega \times$ cm^2.

Fluorescein as paracellular marker in HT-29/B6, but not in Caco-2 cells

To validate fluorescein as a paracellular marker in HT-29/B6 cells, flux and G^{epi} were measured at three different temperatures: 37, 25, and 15°C. The results are presented in Fig. 5 *A* and show that TJ opening at low $[Ca^{2+}]_o$ is clearly temperature-dependent and almost completely blocked at 15°C. In contrast, the relationship between fluorescein flux and G^{epi} is not affected by temperature, indicating that

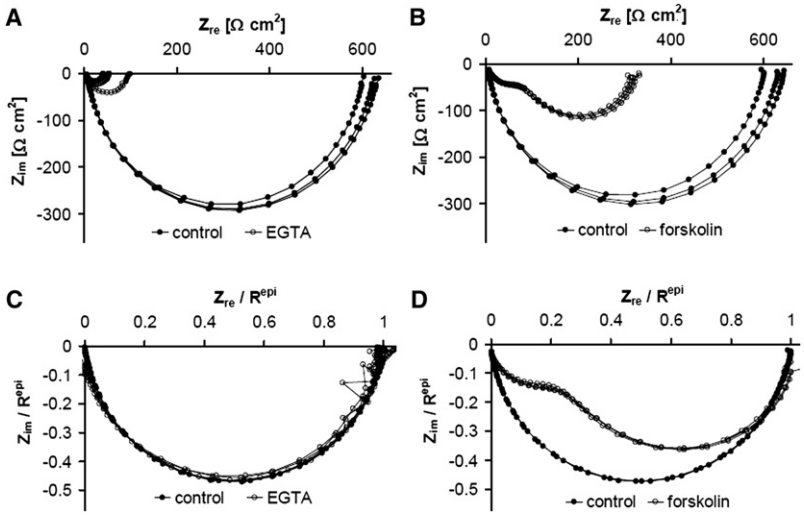

FIGURE 3 Nyquist plot of impedance spectra recorded from a HT-29/B6 cell layer in the absence and presence of EGTA (*A* and *C*) and forskolin (*B* and *D*). (*A*) Parameters (mean ± SE) obtained from the three control spectra are R^{sub}, 5.80 ± 0.13 $\Omega \times$ cm^2; R^{epi}, 615.5 ± 9.4 $\Omega \times$ cm^2; C^{epi}, 4.63 ± 0.03 μF/cm^2. Simultaneously measured fluorescein flux increased from 0.10 ± 0.01 nmol/cm^2/h ($n = 3$) under control conditions by a factor of 20 at an R^{epi}_{-EGTA} of 56 $\Omega \times$ cm^2. This allowed to calculate R^{trans} to 1300 $\Omega \times$ cm^2, $R^{para}_{control}$ to 1170 $\Omega \times$ cm^2 and R^{para}_{EGTA} to 58.5 $\Omega \times$ cm^2 (Eqs. 1 and 2). (*B*) Parameters (mean ± SE) obtained from the three control spectra: R^{sub}, 6.90 ± 0.11 $\Omega \times$ cm^2; R^{epi}, 618.5 ± 12.8 $\Omega \times$ cm^2; C^{epi}, 3.93 ± 0.04 μF/cm^2. The simultaneously measured fluorescein flux remained virtually unchanged (control, 0.31 ± 0.05 nmol/cm^2/h; forskolin 0.26 ± 0.03 nmol/cm^2/h). Without further information, R^{trans} and R^{para} cannot be determined from these data. (*C* and *D*) Same as *A* and *B*, but normalized with respect to R^{epi} to illustrate, that changes in the paracellular pathway (EGTA application, *C*) did not alter the general shape of the curves. In contrast, changing the transcellular pathway by forskolin-induced Cl^- secretion, greatly alters the general shape of the curves (*D*).

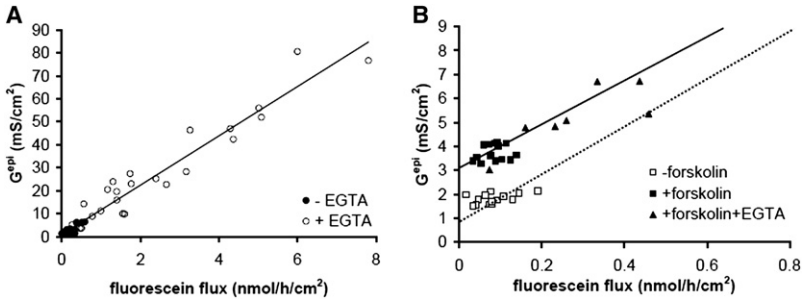

FIGURE 4 G^{epi} versus fluorescein flux plots from experiments on HT-29/B6 cell layers in the absence and presence of EGTA (*A*) and forskolin followed by EGTA (*B*). (*A*) Values obtained in the absence (●) and presence (○) of EGTA fall onto a straight line. G^{trans} estimated from the *y*-intercept: 0.89 mS/cm^2 (R^{trans} = 1120 Ω × cm^2). Line, linear regression; slope 10.7 × 10^6 S × h/mol. (*B*) Values obtained after the application of forskolin (■) are shifted along the *y* axis compared to values obtained under control conditions (□), whereas values in the presence of forskolin and forskolin + EGTA (▲) fall onto a straight line (*solid line*: linear regression, slope 9.1 × 10^6 S × h/mol). This line has a similar slope as the line obtained in the absence of forskolin obtained in *A* (*dotted line*). Thus, in the presence of forskolin, G^{trans} increased to 3.0 mS/cm^2 (R^{trans} = 333 Ω × cm^2).

fluorescein is not actively transported through the cell. Linear regression in Fig. 5 *A* resulted in G^{trans} values of 0.74 mS/cm^2 and 0.99 mS/cm^2 at 37 and 25°C, respectively. At 15°C EGTA failed to affect G^{epi} and fluorescein flux, so that no G^{trans} value could be calculated. In Fig. 5 *B*, the same data are shown, but with flux direction (apical to basolateral and vice versa) indicated instead of temperature. Again, no difference was seen in the relationship between G^{epi} and fluorescein flux, and G^{trans} values of 0.83 mS/cm^2 (apical to basolateral) and 0.61 mS/cm^2 (basolateral to apical) were obtained. In contrast, $^{22}Na^+$ flux clearly depended on the direction of flux (Fig. 5 *C*). When G^{epi} was plotted against Na^+ permeability, values measured in the apical to basolateral direction were shifted to the right, compared to values measured in the basolateral to apical direction. In the latter case, G^{trans} estimated from the *y*-intercept, was comparable to G^{trans} determined from fluorescein flux values (1.05 mS/cm^2), whereas apical to basolateral $^{22}Na^+$ flux data resulted in an apparently negative G^{trans} value (−2.42 mS/cm^2). This is indicative of a transcellular Na^+ transport route in absorptive direction in HT-29/B6 cells (compare Fig. 2 *A*).

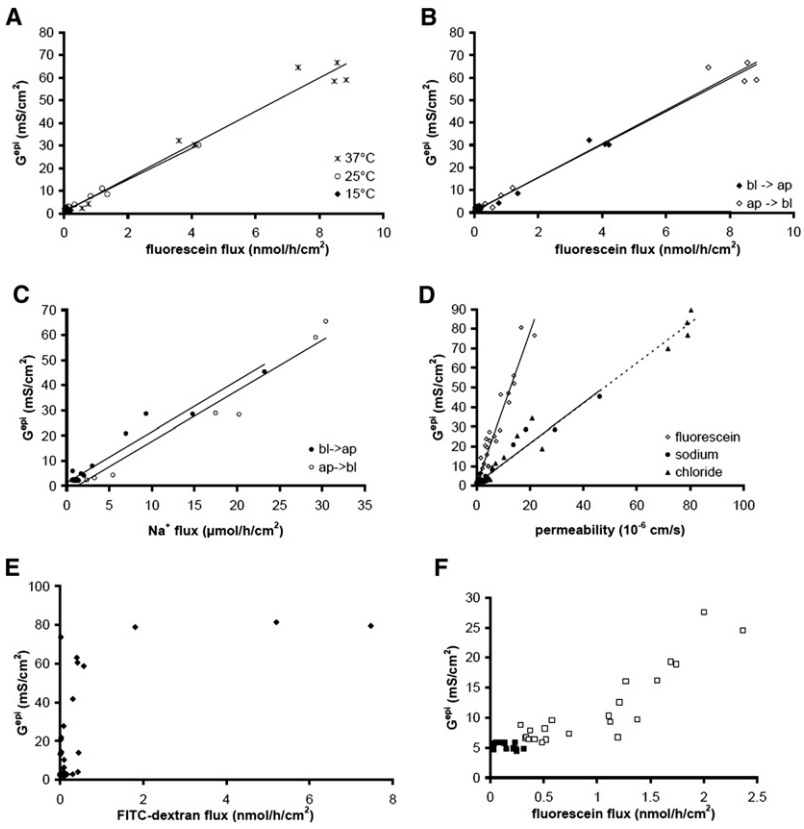

FIGURE 5 (*A*) G^{epi} versus fluorescein flux was independent of temperature in the range of 15°C to 37°C. Line, linear regression; slopes 7.4 × 10^6 S × h/mol (37°C), 7.0 × 10^6 S × h/mol (25°C). (*B*) G^{epi} versus fluorescein flux was independent of the flux direction (basolateral to apical, ◆; apical to basolateral, ◇, slopes of regression lines 7.5 × 10^6 S × h/mol and 7.4 × 10^6 S × h/mol, respectively). (*C*) In contrast, G^{epi} versus Na^+ flux was clearly dependent of the flux direction (basolateral to apical, ●; apical to basolateral, ○). Slopes of regression lines were similar (2.03 × 10^3 S × h/mol and 2.01 × 10^3 S × h/mol, respectively) but values in the apical to basolateral direction were shifted along the *x* axis, indicating a transcellular Na^+ flux under these conditions. G^{trans} calculated from data in the basolateral to apical direction was similar to G^{trans} calculated from fluorescein flux (Fig. 4 *A*) and amounted to 1.05 mS/cm^2 (R^{trans} = 950 Ω × cm^2), whereas in the apical to basolateral direction a calculation of G^{trans} would yield a value of −2.42 mS/cm^2 (R^{trans} = −410 Ω × cm^2). (*D*) Comparison of G^{trans} versus flux of fluorescein (◇), Na^+ (basolateral to apical, ◆) and Cl^- (apical to basolateral, ▲). The *y*-intercepts under these three conditions result in a mean G^{trans} of 0.88 mS/cm^2 (R^{trans} = 1140 Ω × cm^2). The slopes for Na^+ (1.029 × 10^3 S × s/cm^3) and Cl^- flux (1.031 × 10^3 S × s/cm^3) were very similar, indicating, that HT-29/B6 cell layers do not discriminate between these two ions. The slope for fluorescein was larger (3.9 × 10^3 S × s/cm^3), i.e., fluorescein permeability lower, as expected for an ion of larger diameter. (*E*) In contrast to fluorescein, G^{epi} versus 10 kDa FITC-dextran flux did not result in a straight line, indicating that 10 kDa FITC-dextran does not pass through the same paracellular pores as the ions determining paracellular conductance. (*F*) In Caco-2 cell layers G^{epi} versus fluorescein flux (apical to basolateral) did not yield a straight line (values the absence ■ and presence □ of EGTA). Therefore, fluorescein flux should not be used to estimate G^{trans} in these cells.

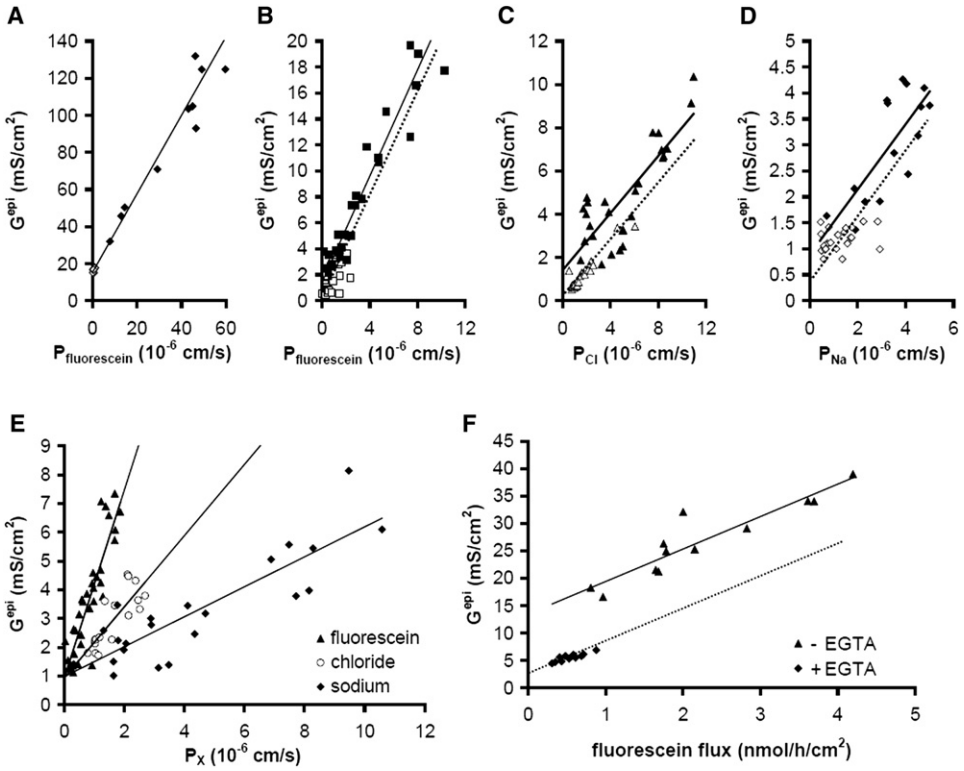

FIGURE 6 (*A*) G^{epi} versus fluorescein permeability plots from experiments on MDCK C11 cell layers. Values obtained in the absence (◇) and presence (◆) of EGTA fall onto a straight line. G^{trans} estimated from the *y*-intercept: 15.4 mS/cm^2 (R^{trans} = 64.9 Ω × cm^2). Line: linear regression, slope 2.12 × 10^3 S × s/cm^3. (*B*) G^{epi} versus fluorescein permeability plots from experiments on MDCK C7 cell layers. Values obtained in the absence of EGTA (□) do not fall onto the same line as those obtained in the presence of EGTA (■). Estimates from the *y*-intercept of the linear regression (*solid line*, slope 2.05 × 10^3 S × s/cm^3) of the values obtained in the presence of EGTA yielded a G^{trans} of 1.44 mS/cm^2, but values in the absence of EGTA lie ~1 mS/cm^2 lower, as judged by shifting the regression line along the *y* axis (*dotted line*). (*C*) G^{epi} versus Cl^- permeability plots from experiments on MDCK C7 cell layers. As in *B*, values obtained in the absence of EGTA (△) lie ~1 mS/cm^2 lower than estimated from a linear regression (*solid line*, slope 0.66 × 10^3 S × s/cm^3) of values obtained in the presence of EGTA (▲). In the presence of EGTA a G^{trans} of 1.41 mS/cm^2 is calculated. (*D*) G^{epi} versus Na^+ permeability plots from experiments on MDCK C7 cell layers. As in *B* and *C*, values obtained in the absence of EGTA (◇) lie ~1 mS/cm^2 lower than estimated from a linear regression (*solid line*, slope 0.63 × 10^3 S × s/cm^3) of values obtained in the presence of EGTA (◆). In the presence of EGTA a G^{trans} of 1.1 mS/cm^2 is calculated. Thus, from *B-D*, the mean G^{trans} in the absence of EGTA amounts to 0.31 mS/cm^2, yielding a R^{trans} of 3230 Ω × cm^2. (*E*) In MDCK C7 cells stably transfected with the paracellular cation pore claudin-10b, a plot of G^{epi} versus fluorescein (▲), Cl^- (○), and Na^+ (◆) permeability yields G^{trans} values of 0.94, 0.93, and 0.98 mS/cm^2, respectively, which have to be corrected by 0.6 mS/cm^2 for values in the absence of EGTA. R^{trans} thus amounts to 2860 Ω × cm^2. The slope of G^{epi} versus Na^+ (0.50 × 10^3 S × s/cm^3) is lower than for Cl^- (1.12 × 10^3 S × s/cm^3) and fluorescein (3.3 × 10^3 S × s/cm^3), mirroring the claudin-10b-induced increased in cation. (*F*) An atypical clone of MDCK II cells stably transfected with claudin-3 clone presented a strongly reduced G^{trans} in the absence of EGTA (◆) whereas in the presence of EGTA (▲), G^{trans} (13.4 mS/cm^2) was comparable to the G^{trans} obtained in control cells shown in *A*. Solid line: linear regression (slope 5.9 × 10^6 S × h/mol); dotted line: regression line shifted along the *y* axis.

$^{36}Cl^-$ flux was measured in the apical to basolateral direction, as HT-29/B6 cells are known to actively secrete Cl^-. As shown in Fig. 5 *D*, G^{trans} (0.71 mS/cm^2) was similar to the values obtained from fluorescein and $^{22}Na^+$ flux experiments. Furthermore, Fig. 5 *D* shows that Na^+ and Cl^- permeabilities in HT-29/B6 cells are very similar. As can be deduced from the larger slope of the regression line, fluorescein permeability is considerably lower than Na^+ and Cl^- permeabilities, however, fluorescein permeability is also proportional to G^{epi} and thus fulfills the criterion for a paracellular marker defined in Eq. 1.

In contrast to fluorescein flux, 10 kDa FITC-dextran flux does not show a linear dependence on G^{epi} (Fig. 5 *E*, exemplary Nyquist diagrams of impedance measurements; see Fig. S2). Below a threshold G^{epi} value of 70 mS/cm^2 HT-29/B6 cell layers are practically impermeable to 10 kDa FITC-dextran, but flux abruptly increases above this threshold. Similar characteristics were obtained with 4 kDa FITC-dextran (not shown). It is concluded that at physiological paracellular resistances FITC-dextran does not pass the cell layer along the same route as the major ions responsible for resistance measurement and therefore, FITC-dextrans are unsuitable as paracellular marker in this context.

It has to be emphasized, however, that the validity of fluorescein as a paracellular marker has to be established for each cell line. Whereas it fulfills all criteria for a paracellular marker in HT-29/B6 cells, it does not in another colonic cell line, Caco-2. In these cells, the relationship between G^{epi} and fluorescein flux in the absence and presence of EGTA was clearly not linear (Fig. 5 *F*).

Fluorescein flux versus G^{epi} in MDCK cells in the absence and presence of EGTA

High resistance MDCK C7 and low resistance MDCK C11 cell layers were used for further testing of the technique presented here (exemplary Nyquist diagrams of impedance measurements; see Fig. S2). In both MDCK subclones, a plot of G^{epi} against fluorescein permeability in the presence of EGTA yielded a straight line (Fig. 6, *A* and *B*), in the case of

MDCK C11 cells with a y-intercept at a G^{trans} of 15.4 mS/cm^2, in MDCK C7 cells with a y-intercept at a G^{trans} of 1.4 mS/cm^2. Thus, MDCK C11 cells differ from MDCK C7 cells not only in R^{para} but also in R^{trans}. Interestingly, the slope G^{epi}/fluorescein permeability, i.e., the fluorescein permeability relative to the permeability of the ions that determine G^{epi}, is very similar for both MDCK C7 and MDCK C11 cell layers (2.05×10^3 S $\times$ s/cm^3 and 2.12×10^3 S $\times$ s/cm^3, respectively). In contrast to HT-29/B6 cells and to MDCK C11 cells, values obtained from MDCK C7 cells in the absence and presence of EGTA did not fall onto one single line. As shown in Fig. 2 *B*, this indicates that in these cells EGTA affected not only R^{para} but also R^{trans}, analogous to the effect of forskolin on R^{trans} of HT-29/B6 cells shown in Fig. 4 *B*. An artifact from the use of fluorescein as a paracellular marker could be ruled out, because Na^+ and Cl^- flux measurements showed the same shift (Fig. 6, *C* and *D*) of ~1 mS/cm^2. It is therefore concluded that G^{trans} in MDCK C7 cells at high $[Ca^{2+}]_o$ is in the order of 0.4 mS/cm^2.

MDCK C7 cells transfected with claudin-10b have been shown recently to exhibit a reduction in R^{epi} due to a strong paracellular cation permeability (4). When these cells were examined in this study, the differences in slope in the plot of G^{epi} against fluorescein, Cl^-, and Na^+ permeability support this finding (Fig. 6 *E*). All three markers yielded the same G^{trans} value of 0.94, 0.93, and 0.98 mS/cm^2, respectively, which in this clone has to be corrected by 0.6 mS/cm^2 to account for the EGTA effect on G^{trans}, but the slope of G^{epi}/Na^+ permeability (0.50×10^3 S $\times$ s/cm^3) was greatly reduced compared to G^{epi}/Cl^- permeability (1.12×10^3 S $\times$ s/cm^3) values, indicating an increased P_{Na}/P_{Cl}. Nyquist diagrams of impedance measurements (compare Fig. S2, *B* and *C*) show the resulting decrease in R^{epi} clearly.

During the selection of stably transfected clones such as the cldn10b expressing MDCK C7 clone, special care has to be taken that the selection process does not favor subclones that differ in their general ion channel or transporter configuration. Fig. 6 *F* shows the usability of this technique for screening such stably transfected cells. Here, a claudin-3-transfected MDCK II subclone is presented with a greatly decreased G^{trans} that, in contrast to control cells, is affected strongly by EGTA. As other claudin-3-transfected clones did not present these properties, this clone was excluded from further studies.

Calculation of R^{para}

In principle, there are two ways to calculate G^{para} (R^{para}): 1), from the fluxes before the application of EGTA and the slope s of the relationship between flux and G^{epi} using Eq. 1; or 2), from the difference between G^{epi} and G^{trans} (Eq. 2). However, the second variant is not recommended as it is more sensitive to data scatter and therefore more error-prone, especially in high resistance epithelia. As illustrated in Fig. 7, for routine evaluation, all values obtained from several single experiments were plotted into one single diagram to check for linearity and potential effects of EGTA on G^{trans}, G^{trans}, and G^{para} were then calculated for each individual experiment (as indicated in Fig. 7 *A*), converted into resistances and averaged to obtain mean data presented in Fig. 7 *B*. Together with the capacity values for each cell line presented in Fig. 7 *C*, and R^{sub} values in the order of 10 $\Omega \times$ cm^2 (Fig. 7), the method presented in this study allows the determination of all components of the electrical circuit depicted in Fig. 1 *B* and thus a quantification of both the para- and the transcellular transport pathway.

DISCUSSION

One-path and two-path impedance spectroscopy

In this study, we describe a condensed impedance model to discriminate between paracellular and transcellular pathways across epithelia. We dubbed this technique two-path impedance spectroscopy to discern it from model assumptions that are even further reduced and solely separate subepithelial from epithelial contributions to barrier function (one-path impedance spectroscopy (e.g., 12–15,32,35)), but also from more complex epithelial models (17,24,25). Although these complex models certainly provide a more detailed and

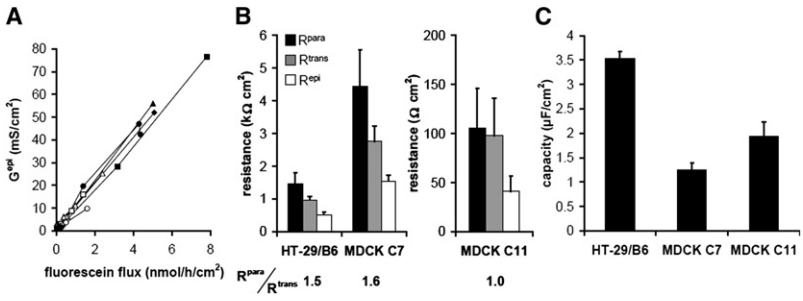

FIGURE 7 (*A*) G^{epi} versus fluorescein permeability plot from experiments on HT-29/B6 cell layers in the absence and presence of EGTA. G^{trans} and G^{para} from different experiments (points joined by lines for clarity; see Fig. S3 for regression lines) can be evaluated separately to obtain mean resistances, if the general plot of all values shows no effects of EGTA on G^{trans}. If, as in MDCK C7 cells, EGTA has an effect on G^{trans}, values have to be corrected (Fig. 6). (*B*) Mean $\pm$ SE of R^{para}, R^{trans}, and R^{epi} calculated from single experiments (HT-29/B6, $n = 8$; MDCK C7, $n = 6$; MDCK C11, $n = 5$) as described in *A*. A ratio $R^{para}/R^{trans} > 1$ indicates a (moderately) tight epithelium (HT-29/B6, MDCK C7), a ratio ≤ 1 a leaky epithelium (MDCK C11). (*C*) Mean $\pm$ SE of the epithelial capacities in HT-29/B6 and MDCK cell layers. Capacity values per unit filter area are significantly higher in HT-29/B6 than in both MDCK C7 and C11 cells ($p < 0.01$, Student's t-test), indicating a stronger increase in surface area in these cells, e.g., through microvilli or membrane invaginations. R^{sub} was similar for all cell types (HT-29/B6, 10.9 $\pm$ 1.4 $\Omega \times$ cm^2; MDCK C7, 11.4 $\pm$ 1.2 $\Omega \times$ cm^2; MDCK C11, 10.7 $\pm$ 1.6 $\Omega \times$ cm^2) and is assumed to primarily reflect the resistance of the filter supports.

accurate description of the electrical properties of epithelia, their handling is complicated and often not apt for routine applications, such as the screening of a large number of epithelial cell layers.

The general approach is based on impedance recordings at 40–50 discrete AC frequencies ranging from ~1 Hz to >10 kHz (12), combined in this study with a manipulation of the paracellular pathway and flux measurements of a paracellular marker. Recordings at low frequencies are equivalent to DC measurements and yield the total epithelial resistance R^t (TER), measurements at the highest frequencies directly yield R^{sub}, and the difference between these two values is equivalent to the epithelial resistance R^{epi}. In cell cultures, R^{sub} is basically the resistance of the filter support, however, this value may differ from the resistance obtained from empty filters, as cells may secrete matrix proteins or may grow into the pore structures of the membranes used. Furthermore, due to the shape and the position of the electrodes, the distribution of the electrical field across a low resistance empty filter membrane may differ from that across a filter covered by a high resistance epithelial cell layer. Thus, for this application, especially at the very low resistances obtained after the application of EGTA, the accuracy of simply measuring empty filter resistance is not sufficient (Fig. 2 *D*).

Limitations

There are three major limitations of the two-path impedance technique presented in this study: 1), the accuracy of R^{sub} determination, especially in low resistance epithelia; 2), the scatter of flux values, especially in high resistance epithelia; and 3), inadequate properties of the marker for paracellular flux.

As discussed above, the importance of an accurate R^{sub} determination increases with decreasing R^{epi}. It is indispensable, therefore, if the Ca^{2+} switch method is used to manipulate R^{para}. This is illustrated by a simple calculation, assuming an R^{sub} of 10 $\Omega \times cm^2$. Failing to take R^{sub} into account will cause an error in G^{epi} of only 3% at an R^t of 300 $\Omega \times cm^2$, but an error of 30% at an R^t of 30 $\Omega \times cm^2$.

Scatter of flux values is predominantly a problem in high resistance epithelia. Here, due to high R^{para}, the paracellular flux is so low that it is often close to the detection limit. Furthermore, at such low paracellular fluxes, even minor transcellular flux fractions start to gain importance.

The choice of the paracellular marker is essential for the validity of the two-path impedance technique. Ideally, the marker should be exclusively transported along the paracellular route, not activate or inhibit any ion-channels or transporters, be electrically uncharged, be detectable at very low concentrations and, preferably, nonradioactive.

The first point is complicated by the fact that there seems to be two different paracellular pathways (29,36–38). Small pores with a diameter of ~0.8 nm allow the passage of all major extracellular inorganic ions (Na^+, Cl^-, HCO_3^-), and the abundance of these pores determines G^{para}. Large pores that have been hypothesized to result either from dynamic TJ strand breaks (38) or to reside in tricellular TJs (29) allow the passage of ions and macromolecules as large as 10–20 kDa. If the strand break hypothesis holds true, part of the observed flux would be independent of G^{para} and thus cause an overestimation of flux values.

In this context, a paracellular marker has to be found that is small enough to pass the small pores, otherwise its flux cannot be proportional to R^{para}. Comparison of Fig. 4 *A* or Fig. 5, *A* and *E*, shows clearly that in HT-29/B6 cells fluorescein fulfills this requirement whereas 10 kDa dextran does not. In HT-29/B6 cells there is no evidence that fluorescein changes the properties of the transepithelial pathway, as normalized impedance curves in the absence and presence of fluorescein are indiscernible. Fluorescein is nonradioactive and can thus be handled without special precautions. Due to its fluorescence properties, it can be reliably detected down to subnanomolar concentrations. The major drawback of fluorescein is that it is doubly negatively charged at pH 7.4 (39). Therefore, flux measurements have to be carried out under voltage-clamp conditions in preparations that build up transepithelial voltages. Depending on the preparations used and on the extracellular pH value, fluorescein may also be transported transcellularly, either according to pH partitioning (Caco-2 cells (40)) or by a proton-coupled monocarboxylic acid transporter (Caco-2 cells (39,41), jejunum but not Caco-2 cells (40)). However, both mechanisms have been reported to be irrelevant a pH 7.4 (40,41).

It is pivotal to test for each preparation whether fluorescein meets all criteria of a reliable paracellular marker. In this study, the validity was shown for HT-29/B6, MDCK C7, and MDCK C11 cells, but not for Caco-2 cells.

Applications

The two-path impedance technique was developed to quantify effects of tight junction proteins when up- or downregulated in epithelial cell lines (28,29). However, it soon proved to be an exceedingly helpful tool for screening different clones during the transfection process, especially during selection of stably transfected clones, as presented in Fig. 6 *F*.

For evaluation of the data, it was advantageous to plot data obtained from several single cell layers into one graph, as this allowed to detect effects such as the reduction of R^{trans} at low $[Ca^{2+}]_o$, that would not have been readily visible if only data from one experiment had been plotted at a time. For the subsequent calculation of R^{trans} and R^{para} as presented in Fig. 7, however, data from each cell layer were then evaluated separately, to reduce the effects of data scatter on R^{trans} and R^{para}.

Two-path impedance spectroscopy could also be used to quantify changes in the transcellular pathway, such as the

activation of Cl^- secretion during the application of forskolin (Fig. 4 *B*) or an activation of TRPV4 channels by the application of 4αPDD (8).

SUPPORTING MATERIAL

Three figures are available at http://www.biophysj.org/biophysj/supplemental/S0006-3495(09)01350-2.

We thank D. Sorgenfrei for technical help and S. Milatz and Dr. S. Andres for providing some of the experimental data.

This study was supported by the German Research Foundation (DFG GU447/11-1 and reseach unit FOR 721) and the Sonnenfeld Stiftung Berlin.

REFERENCES

1. Tsukita, S., M. Furuse, and M. Itoh. 2001. Multifunctional strands in tight junctions. *Nat. Rev. Mol. Cell Biol.* 2:285–293.
2. Ikenouchi, J., M. Furuse, K. Furuse, H. Sasaki, S. Tsukita, et al. 2005. Tricellulin constitutes a novel barrier at tricellular contacts of epithelial cells. *J. Cell Biol.* 171:939–945.
3. Amasheh, S., N. Meiri, A. H. Gitter, T. Schöneberg, J. Mankertz, et al. 2002. Claudin-2 expression induces cation-selective channels in tight junctions of epithelial cells. *J. Cell Sci.* 115:4969–4976.
4. Günzel, D., M. Stuiver, P. J. Kausalya, L. Haisch, S. M. Krug, et al. 2009. Claudin-10 exists in six alternatively spliced isoforms which exhibit distinct localization and function. *J. Cell Sci.* 122:1507–1517.
5. Mankertz, J., and J. D. Schulzke. 2007. Altered permeability in inflammatory bowel disease: pathophysiology and clinical implications. *Curr. Opin. Gastroenterol.* 23:379–383.
6. Fasano, A., and J. P. Nataro. 2004. Intestinal epithelial tight junctions as targets for enteric bacteria-derived toxins. *Adv. Drug Deliv. Rev.* 56:795–807.
7. Tiwari-Woodruff, S., L. Beltran-Parrazal, A. Charles, T. Keck, T. Vu, et al. 2006. K^+ channel KV3.1 associates with OSP/claudin-11 and regulates oligodendrocyte development. *Am. J. Physiol. Cell Physiol.* 291:C687–C698.
8. Reiter, B., R. Kraft, D. Günzel, S. Zeissig, J. D. Schulzke, et al. 2006. TRPV4-mediated regulation of epithelial permeability. *FASEB J.* 20:1802–1812.
9. Günzel, D., S. Amasheh, J. F. Richter, S. Pfaffenbach, J. P. Kausalya, et al. 2009. Claudin-16 affects transcellular Cl^- secretion in MDCK cells. *J. Physiol.* 587:3777–3793.
10. Rajasekaran, S. A., K. W. Beyenbach, and A. K. Rajasekaran. 2008. Interactions of tight junctions with membrane channels and transporters. *Biochim. Biophys. Acta.* 1778:757–769.
11. Van Driessche, W., J. L. Kreindler, A. B. Malik, S. Margulies, S. A. Lewis, et al. 2007. Interrelations/cross talk between transcellular transport function and paracellular tight junctional properties in lung epithelial and endothelial barriers. *Am. J. Physiol. Lung Cell. Mol. Physiol.* 293:L520–L524.
12. Schifferdecker, E., and E. Frömter. 1978. The AC impedance of *Necturus* gallbladder epithelium. *Pflugers Arch.* 377:125–133.
13. Fromm, M., C. E. Palant, C. J. Bentzel, and U. Hegel. 1985. Protamine reversibly decreases paracellular cation permeability in *Necturus* gallbladder. *J. Membr. Biol.* 87:141–150.
14. Bürgel, N., C. Bojarski, J. Mankertz, M. Zeitz, M. Fromm, et al. 2002. Mechanisms of diarrhea in collagenous colitis. *Gastroenterology.* 123:433–443.
15. Zeissig, S., N. Bürgel, D. Günzel, J. Richter, J. Mankertz, et al. 2007. Changes in expression and distribution of claudin-2, -5 and -8 lead to discontinuous tight junctions and barrier dysfunction in active Crohn's disease. *Gut.* 56:61–72.
16. Kottra, G., and E. Frömter. 1984a. Rapid determination of intraepithelial resistance barriers by alternating current spectroscopy: experimental procedures. *Pflugers Arch.* 402:409–420.
17. Kottra, G., and E. Frömter. 1984b. Rapid determination of intraepithelial resistance barriers by alternating current spectroscopy: test of model circuits and quantification of results. *Pflugers Arch.* 402:421–432.
18. Frömter, E., and J. Diamond. 1972. Route of passive ion permeation in epithelia. *Nat. New Biol.* 235:9–13.
19. Cereijido, M., E. Stefani, and A. M. Palomo. 1980. Occluding junctions in a cultured transporting epithelium: structural and functional heterogeneity. *J. Membr. Biol.* 53:19–32.
20. Gitter, A. H., M. Bertog, J. D. Schulzke, and M. Fromm. 1997. Measurement of paracellular epithelial conductivity by conductance scanning. *Pflugers Arch.* 434:830–840.
21. Lewis, S. A., D. C. Eaton, C. Clausen, and J. M. Diamond. 1977. Nystatin as a probe for investigating the electrical properties of a tight epithelium. *J. Gen. Physiol.* 70:427–440.
22. Wills, N. K., S. A. Lewis, and D. C. Eaton. 1979. Active and passive properties of rabbit descending colon: a microelectrode and nystatin study. *J. Membr. Biol.* 45:81–108.
23. Clausen, C., S. A. Lewis, and J. M. Diamond. 1979. Impedance analysis of a tight epithelium using a distributed resistance model. *Biophys. J.* 26:291–318.
24. Păunescu, T. G., and S. I. Helman. 2001. cAMP activation of apical membrane Cl^- channels: theoretical considerations for impedance analysis. *Biophys. J.* 81:838–851.
25. Gitter, A. H., K. Bendfeldt, J. D. Schulzke, and M. Fromm. 2000. Trans-/paracellular, surface/crypt, and epithelial/subepithelial resistances of mammalian colonic epithelia. *Pflugers Arch.* 439:477–482.
26. Bertrand, C. A., D. M. Durand, G. M. Saidel, C. Laboisse, and U. Hopfer. 1998. System for dynamic measurements of membrane capacitance in intact epithelial monolayers. *Biophys. J.* 75:2743–2756.
27. Martinez-Palomo, A., I. Meza, G. Beaty, and M. Cereijido. 1980. Experimental modulation of occluding junctions in a cultured transporting epithelium. *J. Cell Biol.* 87:736–745.
28. Amasheh, S., S. Milatz, S. M. Krug, M. Bergs, M. Amasheh, et al. 2009. Na^+ absorption defends from paracellular back-leakage by claudin-8 upregulation. *Biochem. Biophys. Res. Commun.* 378:45–50.
29. Krug, S. M., S. Amasheh, J. F. Richter, S. Milatz, D. Günzel, et al. 2009. Tricellulin forms a barrier to macromolecules in tricellular tight junctions without affecting ion permeability. *Mol. Biol. Cell.* 20: 3713–3724.
30. Stockmann, M., A. H. Gitter, D. Sorgenfrei, M. Fromm, and J. D. Schulzke. 1999. Low edge damage container insert that adjusts intestinal forceps biopsies into Ussing chamber systems. *Pflugers Arch.* 438:107–112.
31. Gitter, A. H., J. D. Schulzke, D. Sorgenfrei, and M. Fromm. 1997. Ussing chamber for high-frequency transmural impedance analysis of epithelial tissues. *J. Biochem. Biophys. Methods.* 35:81–88.
32. Fromm, M., J. D. Schulzke, and U. Hegel. 1985. Epithelial and subepithelial contributions to transmural electrical resistance of intact rat jejunum, in vitro. *Pflugers Arch.* 405:400–402.
33. Gonzalez-Mariscal, L., R. G. Contreras, J. J. Bolívar, A. Ponce, B. Chávez De Ramirez, et al. 1990. Role of calcium in tight junction formation between epithelial cells. *Am. J. Physiol.* 259:C978–C986.
34. Kreusel, K. M., M. Fromm, J. D. Schulzke, and U. Hegel. 1991. Cl^- secretion in epithelial monolayers of mucus-forming human colon cells (HT-29/B6). *Am. J. Physiol.* 261:C574–C582.
35. Tunggal, J. A., I. Helfrich, A. Schmitz, H. Schwarz, D. Günzel, et al. 2005. E-cadherin is essential for in vivo epidermal barrier function by regulating tight junctions. *EMBO J.* 24:1146–1156.
36. Watson, C. J., M. Rowland, and G. Warhurst. 2001. Functional modeling of tight junctions in intestinal cell monolayers using polyethylene glycol oligomers. *Am. J. Physiol. Cell Physiol.* 281:C388–C397.

37. Tang, V. W., and D. A. Goodenough. 2003. Paracellular ion channel at the tight junction. *Biophys. J.* 84:1660–1673.

38. Anderson, J. M., C. M. Van Itallie, and A. S. Fanning. 2004. Setting up a selective barrier at the apical junction complex. *Curr. Opin. Cell Biol.* 16:140–145.

39. Kuwayama, K., S. Miyauchi, R. Tateoka, H. Abe, and N. Kamo. 2002. Fluorescein uptake by a monocarboxylic acid transporter in human intestinal Caco-2 cells. *Biochem. Pharmacol.* 63:81–88.

40. Berginc, K., S. Zakelj, L. Levstik, D. Ursic, and A. Kristl. 2007. Fluorescein transport properties across artificial lipid membranes, Caco-2 cell monolayers and rat jejunum. *Eur. J. Pharm. Biopharm.* 66: 281–285.

41. Konishi, Y., K. Hagiwara, and M. Shimizu. 2002. Transepithelial transport of fluorescein in Caco-2 cell monolayers and use of such transport in in vitro evaluation of phenolic acid availability. *Biosci. Biotechnol. Biochem.* 66:2449–2457.